Journal of Advanced Research (2016) 7, 225–232

Cairo University

Journal of Advanced Research

ORIGINAL ARTICLE

Anode optimization for miniature electronic brachytherapy X-ray sources using Monte Carlo and computational fluid dynamic codes

Masoud Khajeh [a], Habib Safigholi [b,*]

[a] Department of Mechanics, Marvdasht Branch, Islamic Azad University, Marvdasht, Iran
[b] Department of Electrical Engineering, College of Engineering, Shiraz Branch, Islamic Azad University, Shiraz, Iran

ARTICLE INFO

Article history:
Received 21 November 2014
Received in revised form 14 April 2015
Accepted 15 April 2015
Available online 20 April 2015

Keywords:
Electronic brachytherapy
Target
Monte Carlo
Computational fluid dynamic
TG-43U1

ABSTRACT

A miniature X-ray source has been optimized for electronic brachytherapy. The cooling fluid for this device is water. Unlike the radionuclide brachytherapy sources, this source is able to operate at variable voltages and currents to match the dose with the tumor depth. First, Monte Carlo (MC) optimization was performed on the tungsten target-buffer thickness layers versus energy such that the minimum X-ray attenuation occurred. Second optimization was done on the selection of the anode shape based on the Monte Carlo in water TG-43U1 anisotropy function. This optimization was carried out to get the dose anisotropy functions closer to unity at any angle from 0° to 170°. Three anode shapes including cylindrical, spherical, and conical were considered. Moreover, by Computational Fluid Dynamic (CFD) code the optimal target-buffer shape and different nozzle shapes for electronic brachytherapy were evaluated. The characterization criteria of the CFD were the minimum temperature on the anode shape, cooling water, and pressure loss from inlet to outlet. The optimal anode was conical in shape with a conical nozzle. Finally, the TG-43U1 parameters of the optimal source were compared with the literature.

Introduction

In recent years efforts have been made to use miniature electronic brachytherapy X-ray sources (MEBXS) in radiotherapy treatment without radionuclide seed sources. The heart of the MEBXS is a miniature X-ray tube which is very small in dimensions (a small accelerator). Using electrically generated X-rays a radiation dose is delivered at a distance of up to a few centimeters by intracavitary, intraluminal or interstitial application, or by applications with the source in contact with the body surface or very close to the body surface [1–4]. The

* Corresponding author. Tel.: +98 71 3641 0040; fax: +98 71 3641 0068.
E-mail address: safigholi@gmail.com (H. Safigholi).
Peer review under responsibility of Cairo University.

Production and hosting by Elsevier

http://dx.doi.org/10.1016/j.jare.2015.04.006
2090-1232

initial theory of electronic X-ray source is based on the electron bombardment of transmission-type target in a small vacuum tube with low energy electrons and bremsstrahlung photons production. MEBXS have several advantages over conventional radioactive sources. Since the source is a miniature accelerator, with changing voltage (30–60 keV) and currents, it can give desired dose rate to the cancerous tissue. Because low voltages and currents are used, minimal shielding is required and radiation exposure to the staff can be reduced [2–4].

Three companies developed the electronic sources: The Esteya® Electronic Brachytherapy System (Esteya EBS, Elekta AB-Nucletron, Stockholm, Sweden) [5], the INTRABEAM™ Photon Radiosurgery Device by Carl Zeiss Surgical (Oberkochen, Germany), and the Axxent® Electronic Brachytherapy System by Xoft Inc. (Fremont, CA) which developed the MEBXS units for brachytherapy treatment. In 2013 the Esteya brachytherapy mobile system was applied for skin brachytherapy; however, the anode material of target is confidential, and oil cooling system is used for target cooling. The source is outside the patient. In the Carl Zeiss mobile source, electrons are produced by an electron gun outside patient and accelerated to a very fine tube which is in turn attached to a hemisphere gold target at tube tip [2–5]. A thin thickness of beryllium covers the outside surface of target as a thermal buffer. The anode is placed adjacent to tumor for irradiation. The Xoft electronic source is constructed of a disposable micro-layer of tungsten target on an yttrium substrate used as a buffer layer. The target probe is inserted into a flexible plastic sheath, and the water is then pumped around the target to reduce heating from the target [2]. As the MEBXS are novel techniques in brachytherapy treatment, there is potential to improve the design of the anode and the buffer of electronic sources in brachytherapy techniques. The target and buffer thicknesses are significant factors of the X-ray generation process and heat production at the target assembly when electrons decelerate within target. Most of the energy of the electrons is converted to heat in the target (more than 99.8%) and only a very small amount of incident electron energies produce X-rays. There are a few studies on heat analysis in X-ray anodes [6]; however, an overall study for MEBXS on increasing more X-ray production and on the heat analysis of the target assembly cooling was not yet performed.

In this research the Monte Carlo (MC) particle transport code MCNP5 code, was used to optimize the tungsten anode thickness and shapes [7]. Moreover, the OpenFOAM Computational Fluid Dynamic (CFD) simulations code was used to characterize the thermal analysis design of anode (target and buffer) and nozzle design for the MEBXS [8]. Finally, parameters that affect the TG-43U1 dose distribution [9] such as target shape and thickness and target buffer layer were evaluated.

Methodology

TG-43U1 AAPM protocol

The American Association of Physicists in Medicine (AAPM) Task Group 43 published a brachytherapy protocol for dose calculation around brachytherapy sources which was updated to TG-43U1 in 2004 [9,10]. The expression for calculation of 2D dose distribution surrounding brachytherapy source is as shown below:

$$\dot{D}(r,\theta) = S_K \cdot \Lambda \cdot [(G_L(r,\theta)/G_L(r_0,\theta_0)) \cdot g_L(r) \cdot F(r,\theta)]$$

where S_K is the air kerma strength, Λ is the dose rate constant, $G_L(r,\theta)$ is the source geometry function, $g_L(r)$, is the radial dose function, and $F(r,\theta)$ is the two-dimensional anisotropy function. TG-43U1 guidelines for radionuclide sources apply equally well to the MEBXS with two modifications [2,3]. First, S_K must be normalized to beam current because the MEBXS dose rate can easily vary by changing the beam current. Second, anisotropy functions can be approximated as a point-source for the geometry function when the MEBXS active length is close to zero.

Monte Carlo and computational fluid dynamic calculations

The MCNP5 code was used for optimization of more X-ray productions in all simulations [7]. The cross-section data are all derived from the ENDF/B-VI.8 data library. The MEBXS were modeled for three initial anode geometries: cylindrical, hemispherical and conical-hemisphere, whose characteristics are varied in the optimization process, with dosimetric data as recommended by TG-43U1. Details of the final MC geometries simulations of MEBXS are shown in Fig. 1. To reduce MC calculation time, the energy cutoff for electrons outside of and inside of the source is considered 20 and 1 keV, respectively [3]. In addition, the low energy cutoff for photon transport in simulations was 1 keV. ITS-style energy indexing on the DBCN card (Debug Information Card), was used as it is more accurate than the default MCNP-style energy index [3]. Simulations were performed for electron and photon transports in spherical liquid water phantom with a radius of 20 cm and density of 1 g/cm^3 for electron energies of 30–60 keV at polar angles of 0–180° and radial distances from 0.5 to 7 cm [10].

The Computational Fluid Dynamic (CFD) OpenFOAM code was used to characterize the heat analysis of the anode shapes. OpenFOAM is a free, open source CFD software package developed by OpenCFD Ltd. at ESI Group [8]. To characterize the anode, various buffer thickness and shapes, different nozzle shapes and dimensions were changed. Axial symmetric model with field flow is simulated for all cases due to axial symmetric of the MEBXS. The laminar water flow as a cooling fluid circulates around anode at catheter at inlet with average velocity of 0.2 m/s, and 298 K temperature. The water flow rate and operating pressure for cooling system were considered 25 cm^3/min and 3.5 bar, respectively [3]. No slip conditions are assumed for wall boundary. The water dynamic viscosity as a function of temperature, is imported to the CFD code [11]. The water density, specific heat, and thermal conductivity were 998 kg/m^3, 4200 J/kg K and 0.6 W/m K, respectively. The values for Be layer considered were 1844 kg/m^3, 1925 J/kg K, 216 W/m K, respectively. The corresponding values for catheter plastic layer for cooling layer were, 1160 kg/m^3, 1110 J/kg K, and 0.2 W/m K, respectively.

The equations for incompressible fluid flow are used for all simulations. Thus, the governing fluid flow equations include continuity, momentum (Navier–Stokes) and energy equations [12]. The equations are solved by Semi Implicit Pressure

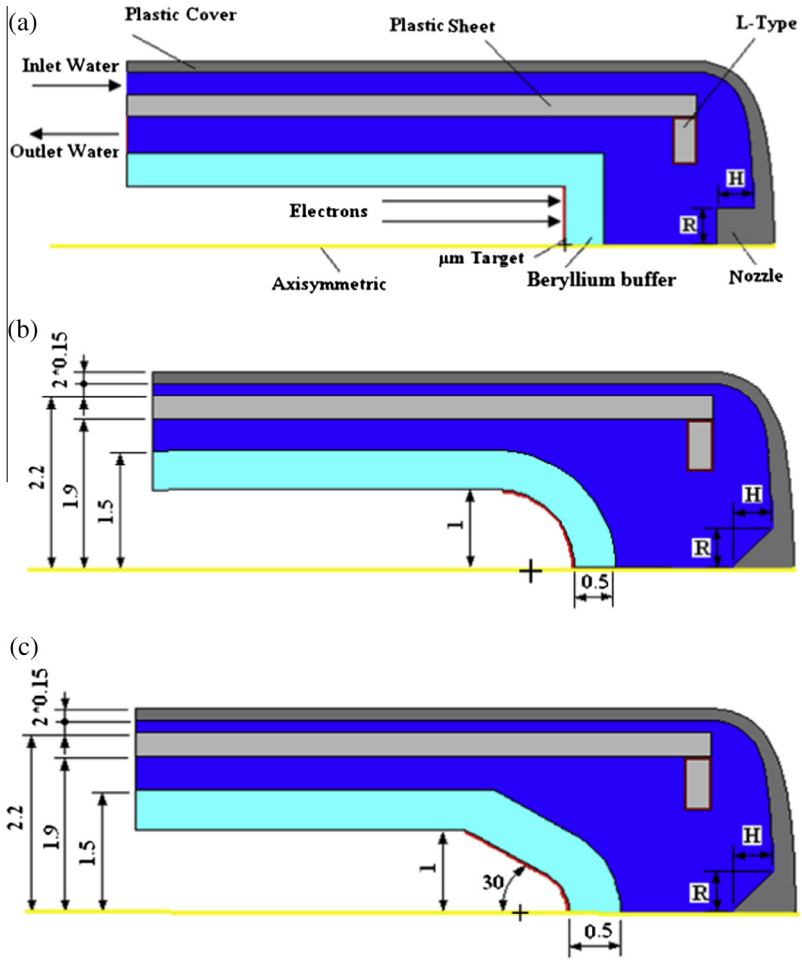

Fig. 1 Different anode shapes and nozzles. (a) Cylindrical anode and nozzle. Components are defined in this figure. (b) Spherical anode with conical nozzle. (c) Final optimal MEBXS are conical anode and nozzle. The half angle of the cone apex is 30°. The dimensions are in millimeters. The dimensions in (a), are the same as in (b and c). R and H are equal to 0.75 mm and represent radius and height of the nozzle shapes, respectively. The μm target surface on the inner surface of beryllium is shown with red color. The origin to derive the TG-43 parameters is shown with sign of +.

Linked Equations (SIMPLE) and Second Order Upwind discretization approaches [13].

Monte Carlo optimization of target-buffer thickness and shape

In this research, the thin thickness of tungsten target layer that is supported by a thicker beryllium buffer layer (Fig. 1) is optimized as an anode layer. To determine the target optimized thickness, the depth of electron penetration in different layers of target materials and buffer is obtained in range of 30–80 keV. The F_5 (photon/cm^2) tally is placed in front of target for different target thicknesses to obtain optimized target thickness. The electron source beam was a uniform cylinder shape with radius of 0.9 mm, located 1 cm from the surface of target [3]. The target is first considered as disk shape with different thicknesses, each having a 2 mm diameter [3]. The target thickness is changed from close to zero to several times (μm) to evaluate the electron penetration depths. The optimized target thickness is a substrate for the beryllium support layer with different thicknesses, and then the effect of the X-ray attenuation is also considered. On the other hand, the thickness target and beryllium support with an emphasis on maximizing the X-ray generated from the anode while reducing the X-ray self-absorption have been optimized. These optimized thicknesses were then evaluated for other anode geometries such as hemispherical and conical shapes (Fig. 1a and b). For targeting conical shapes the apex angle is considered 60° [2,3]. For each run, 10^8 electron histories were simulated in order to have statistical uncertainty lower than 2.5%.

The criteria optimization for target shape was versus of TG-43 $F(r, \theta)$. (1) This function should have minimum variation rather than unity for radial distances between 1 and 7 cm and an angular range of 0–170° in 10° increments. (2) $F(r, 0°)$ should be unity and/or slightly more than unity, since the dose distribution in MEBXS is a little forward peaked. These conditions were the criteria optimization for selection of the anode shape.

Anode characterization by computational fluid dynamic

The heat transfer for anode shapes, buffer thicknesses, various nozzle shapes was investigated. For all investigations in this part, energy was assumed 50 keV which is put onto the target

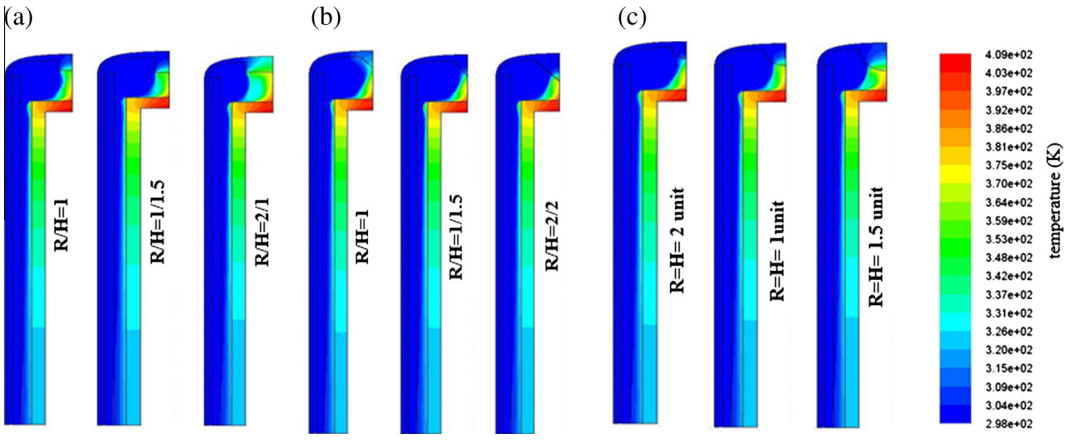

Fig. 2 Temperature distribution (K) for cylindrical buffer-target and (a) cylindrical nozzle, (b) conical nozzle, (c) spherical nozzle, with different radius (R), and height (H) for nozzle. The viscosity of water as a function of temperature is considered to these simulations [11]. The buffer thickness is assumed 0.5 mm. The unit of the temperature labels is K.

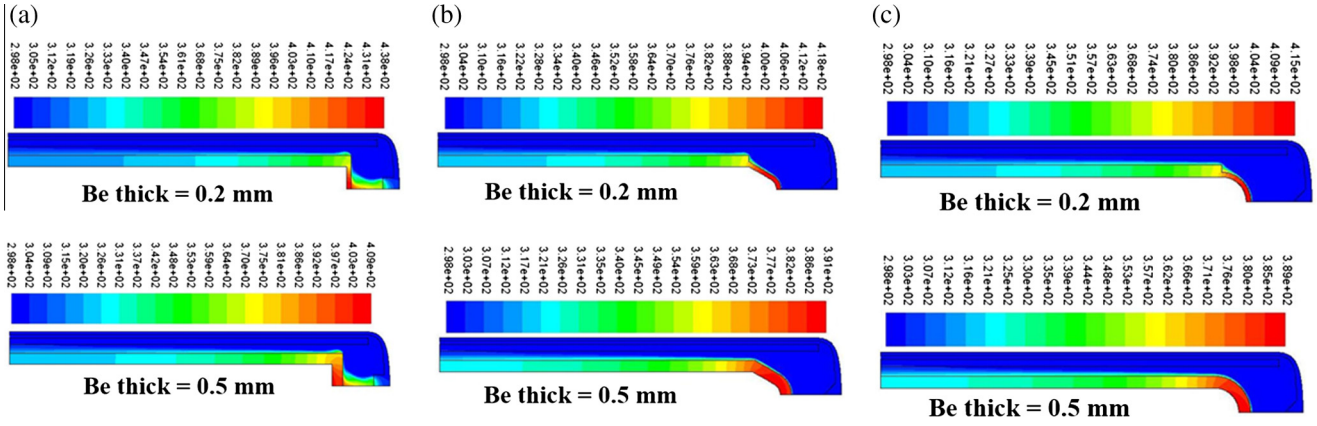

Fig. 3 Temperature distribution (K) for different beryllium thicknesses for (a) cylindrical buffer and nozzle, (b) conical buffer and nozzle, (c) spherical buffer and conical nozzle. The viscosity of water as a function of temperature is considered to these simulations [11]. (b and c) (0.5 mm Be) show the final temperature for the final design of target and buffer shapes. The unit of temperature labels is K.

surface versus W/cm^2. The operating current was 300 μA. Firstly, various nozzle geometries such as cylindrical, spherical, and conical shapes for cylindrical buffer shape were investigated. The buffer thickness was assumed to be 0.5 mm for this investigation (Fig. 1). The unit height and radius of plastic nozzle were selected 0.5 mm ($H = R = 0.5$ mm) for all nozzle shapes. The results were achieved for dimensionless R/H ratio. Fig. 2 shows the temperature distributions (K) for cylindrical target-buffer and different nozzle shapes. Secondly, the effect of beryllium buffer thicknesses with cylindrical, spherical, and conical shapes on the temperature distribution of buffer and cooling water was considered. Fig. 3 shows the temperature distribution (K) for various thicknesses of buffer with different shapes and thicknesses. Moreover, by adding a plastic L-type shape to the end of plastic sheet with different lengths, the effects of the cooling water flow on the anode shapes are considered. Fig. 1 shows the L-type Piece. Finally, by combining the MC optimized target and buffer shapes and CFD characterization for minimum temperature of anode and cooling water, optimal anode shapes for MEBXS were determined. This optimization considered maximizing the X-ray intensity and minimizing the anode temperature. TG-43U1 radial and anisotropy functions of optimized target shapes are compared with the published data by Rivard et al. [2].

Results and discussion

Monte Carlo optimization of target and buffer thicknesses

Fig. 4a shows target thickness versus X-ray intensity for tungsten target. The optimized thickness at 40 keV for target was obtained as 1 μm. In thickness lower than 1 μm, most of the electrons were passed through the target and X-ray generation was low, while in optimized thickness the X-ray intensity is maximized. In thicknesses that are thicker than the "optimized thickness" the output intensity is decreased due to the photon self-absorbing factor in target layer. Table 1 presents tungsten optimized thickness as a function of electron energy which agrees well with the published data in Ref. [6].

Moreover, the X-ray attenuation by different beryllium buffer thicknesses is considered. For 50 keV and 1.45 μm target, the effect of the beryllium buffer thickness on the X-ray

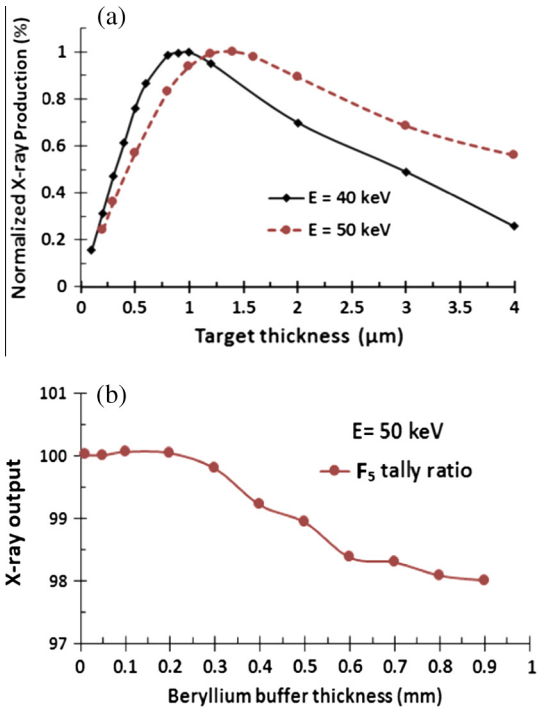

Fig. 4 (a) Normalized X-ray production versus tungsten thickness target for 40 and 50 keV. The F_5 tally (photon/cm^2) was used for calculation. The MC uncertainty was less than 1% for energy range of 30–80 keV. (b) Effect of the beryllium thickness on the X-ray attenuation for 50 keV. The ratio of the F_5 tally (photon/cm^2) with or without beryllium layer determined attenuation quantity.

Table 1 Optimal Tungsten target thickness as a function of electron energy.

E (keV)	Optimal thickness (μm)
30	0.65
35	0.85
40	1.02
45	1.25
50	1.45
60	1.95
80	3.00

intensity attenuation is shown in Fig. 4b. The X-ray attenuation by beryllium buffer is negligible (2% for 1 μm); however, other publications indicate 0.5 mm beryllium is adequate as a buffer [6,14] for these applications.

The optimization criterion for target shape is that the anisotropy functions should be unity and/or slightly more than unity, since the dose distribution in MEBXS is a little forward peaked. Fig. 5, shows the TG-43U1 anisotropy functions for cylindrical, spherical, and conical target shapes for 40 keV. Cylindrical anode shape shows large deviations for $F(r, \theta)$ from unity in the forward (0–90°) and backward (90–170°) directions, while for spherical and conical anode shapes corresponding values are much smaller, and are close to unity. This is due to the electron bombardment of cylinder target is at 90° angle which produces different photon distribution than the conical and spherical targets, and also more photon

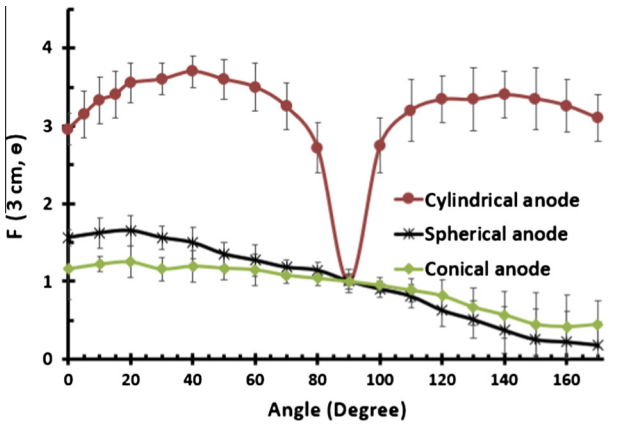

Fig. 5 TG-43U1 anisotropy functions for cylindrical, spherical, and conical target shapes at 3 cm distance. The optimal anisotropy function should be close to unity. The MC uncertainty is less than 2%.

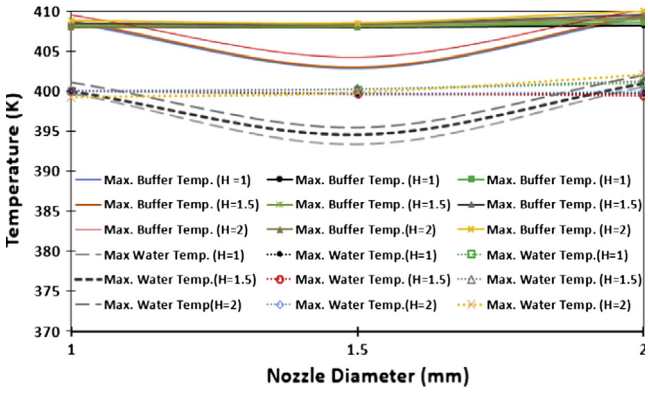

Fig. 6 Temperature of buffer and cooling water for cylindrical, spherical, and conical nozzle shapes with different values of D (diameter), and H (Height). Minimum temperatures were for $R = H = 1.5$.

attenuation is occurred in target at 90° detector for TG-43 anisotropy function. $F(r, \theta)$ are much closer to 1 for the conical anode than those obtained with the hemispherical anode [2]. MC results show that the optimal anode shape is conical target based on optimized target, dose uniform, and 2D anisotropy.

Anode characterization by computational fluid dynamic

Temperature of the 0.5 mm cylindrical buffer with cylindrical, spherical, and conical nozzle shapes (Fig. 2) is presented in Fig. 6. Maximum temperature of beryllium buffer and maximum temperature of cooling water for different R/H ratios are obtained. For all nozzle shapes, the buffer temperature is 10 K higher than the cooling water fluid. In cylindrical nozzle shape for all H values, the temperature differences between buffer and fluid are less than 2 K, while the corresponding values are very well matched for spherical and conical nozzle shapes, and differences are less than 1 K. Minimum temperature corresponds with cylindrical nozzle shape for $R = H = 1.5$. This is due to the return flow between nozzle and buffer for cylindrical nozzle, which is more than spherical

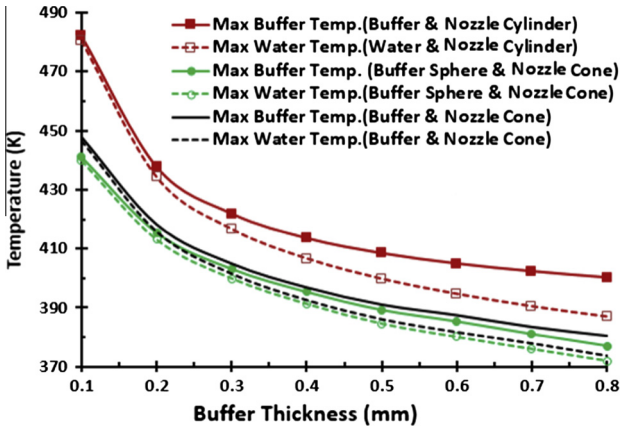

Fig. 7 Temperature as a function of buffer thickness for various shapes. These data are taken for $D = H = 1$. The minimum temperature has occurred for spherical buffer with conical nozzle. The mean difference between max buffer and water temperatures for conical nozzle with spherical and conical buffer shapes is less than 2.5%.

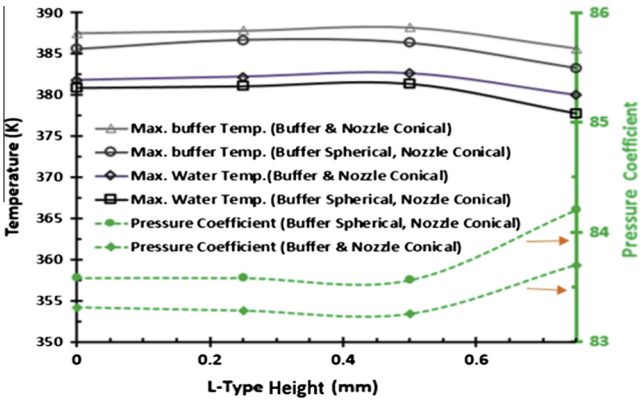

Fig. 8 Buffer and water temperatures versus different L-type heights of plastic sheet for conical and spherical anode shapes. The vertical axis in the left side hand of the curve shows the pressure coefficient of inlet and outlet fluid on the plastic sheet for different lengths of L-type plastic sheet. The pressure coefficient is a non-dimensional quantity which is obtained from the equation of $C_p = \frac{P-P_0}{1/2\rho V^2}$. In this relation, P is absolute pressure, P_0 is a work pressure, ρ is density, and V is the fluid velocity. The buffer thickness is considered 0.5 mm.

and conical nozzle shapes, although the maximum pressure loss between inlet and outlet of fluid has occurred for cylindrical buffer and nozzle shapes due to wall sheer stress and path length of fluid [12]. This shows that the cylindrical buffer and nozzle shapes are not the optimum shapes. In addition, the MC results (Fig. 5) indicate the cylindrical anode is not acceptable.

The maximum temperature as a function of buffer thickness variation with cylindrical, spherical, and conical shapes (Fig. 3) is presented in Fig. 7. The maximum temperature of water means the water temperature on buffer surface. The results show that temperature is decreased, by increasing the buffer thickness. One can conclude the maximum decrease is for spherical buffer and conical nozzle. However, the temperature differences between spherical buffer with conical nozzle and conical buffer and nozzle shapes are less than 2 K.

It is important to note that the average temperature of water in the coolant layer for treatment of patient should be between 297 and 308 K [3]. Fig. 3b and c presents the temperature for optimized buffer thickness (0.5 mm), and final shapes. These figures show the average cooling water temperature surrounding the source is between 298 and 303 K.

The operating pressure of the device is 3.5 bar, in which up to 412 K there is not any water phase to vapor [3,12]. For cylindrical buffer and nozzle shapes with buffer thickness of 0.1–0.2 mm, for conical nozzle and spherical buffer shapes with buffer thickness of 0.1 mm, and for conical buffer and target shapes with buffer thickness of 0.1 mm, the few number of calculation cells shows phase shift. This phase shift was local and the fluid returns immediately to liquid phase when far from the condensed points. This number of limit phase changes was for non-optimized buffer thickness. For optimized buffer thickness (0.5 mm) there is not any phase shift.

Figs. 6 and 7 show that, with a proper fluid flow around the source, the maximum temperature of the device can be reduced. To reduce the buffer temperature, the L-type plastic shape is added to the end of the plastic sheet. Results from different L-type heights with 0.5 mm buffer thickness for spherical and conical anode shapes are presented in Fig. 8. This figure shows, temperature and pressure coefficients for different L-type lengths. The water pressure coefficient is a non-dimensional quantity, which is obtained from the following equation:

$$C_p = \frac{P - P_0}{1/2\rho V^2} \tag{2}$$

In this relation, P is absolute pressure, P_0 is a work pressure, ρ is density, and V is the fluid velocity. This relation shows that the pressure falls off in the coolant layer from inlet to outlet (11).

For L-type height from 0 to 0.5 mm, maximum temperature is increased for two anode shapes (less than 1 K); however, for longer L-type height the maximum temperature is decreased. Spherical buffer with conical nozzle shows the minimum temperature (377 K). However, the minimum pressure loss between inlet and outlet of fluid occurred for conical buffer with conical nozzle. The temperature difference between conical and spherical anode shapes is less than 3 K. The Combination of minimum temperature of buffer-target by minimum pressure difference and MC optimized TG-43U1 anisotropy function, indicates that the optimal design is the conical anode with conical nozzle shapes. On the other hand the conical nozzle shape produces better cooling factor than the spherical shape. The L-type plastic sheet can reduce buffer temperature (up to 3 K) if the construction of the L-type is possible.

TG-43U1 functions for optimal anode shapes

Final TG-43U1 radial dose functions and 2 dimensional anisotropy function of the optimal anode shape (conical) for 50 keV are presented in Table 2. The results were compared with published data by Rivard et al. [2]. The ratios are also presented. The maximum difference between MC radial dose function and published data in Ref. [2] is less than 8%. The

Table 2 MC calculation of TG-43U1 radial dose, $MC_{g(r)}$, and anisotropy function, $MC_{F(3cm,\theta)}$, for MEBXS at 50 keV compared with results of Rivard et al. (Ref. [2]). Also a comparison of the results by Rivard et al. (Ref. [2]), is shown as the *g*-ratio and *F*-ratio. The *MC* uncertainty is at most 2.5%.

r (cm)	$MC_{g(r)}$	Ref. [2]$_{g(r)}$	*g*-ratio	θ (°)	$MC_{F(3cm,\theta)}$	Ref. [2]$_{F(3cm,\theta)}$	*F*-ratio
0.5	1.480	1.418	1.044	0	1.121	1.038	1.079
0.7	1.280	1.211	1.057	10	1.130	1.042	1.084
1	1.000	1.000	1.000	20	1.123	1.047	1.070
1.5	0.720	0.780	0.923	30	1.103	1.035	1.063
2	0.621	0.641	0.969	40	1.141	1.078	1.058
2.5	0.503	0.544	0.925	50	1.160	1.095	1.059
3	0.431	0.470	0.917	60	1.161	1.091	1.063
3.5	0.382	0.411	0.929	70	1.140	1.072	1.063
4	0.342	0.362	0.945	80	1.091	1.041	1.047
4.5	0.299	0.322	0.929	90	1.000	1.00	1.000
5	0.266	0.286	0.930	100	0.954	0.95	1.000
5.5	0.236	0.256	0.922	115	0.896	0.855	1.041
6	0.211	0.229	0.921	130	0.752	0.697	1.076
6.5	0.192	0.206	0.932	145	0.535	0.488	1.096
7	0.171	0.185	0.924	160	0.359	0.329	1.091

corresponding values for anisotropy function are less than 9% which shows good agreement. These differences are due to the anode material which is a combination of the tungsten, yttrium, and silver in the reference data [2].

Uncertainty analysis

As indicated in the TG-43U1 and TG-138 recommendations, the total MC uncertainties are the quadrature sum of the MC uncertainties of dose parameters, cross sections, and source geometry [10,15]. The MC uncertainties for the radial dose function of the final optimized anode (Conical target, conical nozzle, and L-type) are 0.2% at 1 and 2% at 7 cm, respectively. The corresponding values for dose anisotropy function are at most 0.4% and 2.5% at 1 and 7 cm, respectively. Also the MC cross section uncertainties are less than 2.5% [7]. There are MC uncertainties associated with target thickness or source geometry. Typical variation of dose, and 2D dose anisotropy functions for thickness target variations of 1.45 μm ± 10% for 50 keV are calculated. Maximum dose and 2D dose anisotropy uncertainties at 4 cm radial distance for 1 μm + 10% were 4% and 2%, respectively. The corresponding values for 1 μm − 10% were 3% and 2.5%, respectively. The total MC uncertainties were 3.5% and 5.2% at 1 and 7 cm, respectively.

CFD uncertainties associated with buffer thickness variations are calculated. The optimized buffer thickness of Be is 0.5 mm. The effect of the 0.5 mm ± 10% variation for maximum water and buffer temperatures was evaluated. The maximum water and buffer temperatures for 0.5 mm − 10% Be were 392.7 K, and 396.9 K, respectively. The corresponding values for 0.5 mm + 10% Be were 381.5 K, and 387.5 K, respectively. The uncertainty of the water flow rate was calculated for 25 cm^3/min ± 6.25 cm^3/min. For flow rate of 31.25 cm^3/min, the maximum temperatures of cooling water, buffer, and pressure coefficient were 380 k, 372 K, and 67.3 K, respectively. These values for 18.75 cm^3/min were, 392 K, 385 K, and 110.5, respectively. Also the effect of the constant dynamic viscosity (0.001 kg/m s), in comparison with viscosity as a function of temperature was calculated. The results show that, the maximum temperature of water and buffer for all simulation cases reduced (about 10°) when the viscosity is considered as a function of temperature.

Conclusions

In this research, different anode and nozzle shapes were simulated for MEBXS by using the MC MCNP5 and CFD OpenFOAM codes to obtain the optimal design of MEBXS anode. The optimization criteria by MC and CFD codes were the TG-43U1 dose uniform, anisotropy functions close to unity and minimum temperature of the anode shape, respectively. Parameters that affect X-ray intensity and temperature distribution such as target-buffer thickness, shapes, and nozzle shapes were investigated. The optimal anode shape was obtained for conical anode with conical nozzle shapes. Moreover, the L-type edge of the plastic sheet has no significant effect on the TG-43U1 parameters and minimum temperature of the anode. The final optimal anode was in a good agreement compared to the published TG-43U1 parameters of the MEBXS.

Conflict of Interest

The authors have declared no conflict of interest.

Compliance with Ethics Requirements

This article does not contain any studies with human or animal subjects.

Acknowledgments

This research was partially supported by the Grant No. 89/6415 at Marvdasht Branch, Islamic Azad University, Marvdasht, Iran. We also thank Dr. Abraam Soliman from Sunnybrook Health Sciences Centre of Canada and Dr. Dae

Yup Han from University of California at San Diego for the edition of manuscript.

References

[1] Thomadsen BR, Biggs PJ, DeWerd LA, II CWC, Chiu-Tsao ST, Gossman MS, Coffey II CW, et al. Report of AAPM task group 152: model regulations for electronic brachytherapy. AAPM; 2009.
[2] Rivard MJ, Davis SD, DeWerd LA, Rusch TW, Axelrod S. Calculated and measured brachytherapy dosimetry parameters in water for the Xoft Axxent X-ray source: an electronic brachytherapy source. Med Phys 2006;33(11):4020–32.
[3] Safigholi H, Faghihi R, Jashni SK, Meigooni AS. Characteristics of miniature electronic brachytherapy X-ray sources based on TG-43U1 formalism using Monte Carlo simulation techniques. Med Phys 2012;39(4):1971–9.
[4] Karimi Jashni H, Safigholi H, Meigooni AS. Influences of spherical phantom heterogeneities on dosimetric characteristics of miniature electronic brachytherapy X-ray sources: Monte Carlo study. Appl Radiat Isot 2015;95(1):108–13.
[5] Garcia-Martinez T, Chan JP, Perez-Calatayud J, Ballester F. Dosimetric characteristics of a new unit for electronic skin brachytherapy. J Contemp Brachytherapy 2014;6(1):45–53.
[6] Ihsan A, Heo SH, Cho SO. Optimization of X-ray target parameters for a high-brightness microfocus X-ray tube. Nucl Instrum Meth Phys Res B 2007;264(2):371–7.
[7] MCNP-5 Monte Carlo Team. MCNP – A General Monte Carlo N-Particle Transport Code, Version 5. Los Alamos National Laboratory, Los Alamos, NM; 2003.
[8] The Open Source Computational Fluid Dynamic ToolBox OpenFOAM® website. <http://www.openfoam.com> (April, 2014).
[9] Nath R, Anderson LL, Luxton G, Weaver KA, Williamson JF, Meigooni AS. Dosimetry of interstitial brachytherapy sources: recommendations of the AAPM radiation Therapy Committee Task Group No.43 American Association of Physicists in Medicine. Med Phys 1995;22(2):209–34.
[10] Rivard MJ, Coursey BM, DeWerd LA, Hanson WF, Huq MS, Ibbott GS, et al. Update of AAPM Task Group No. 43 report: a revised AAPM protocol for brachytherapy dose calculations. Med Phys 2004;31(3):633–74.
[11] <http://www.engineeringtoolbox.com/water-dynamic-kinematic-viscosity-d_596.html>. [accessed 01.02.15].
[12] Potter MC, Wiggert DC, Ramadan B, Shih TI-P. Mechanics of fluids. 4nd ed. Global Engineering; 2011.
[13] Patankar SV. Numerical heat transfer and fluid flow. New York: McGraw Hill Book Company; 1980.
[14] Beatty J, Biggs PJ, Gall K, Okunieff P, Pardo FS, Harte KJ, et al. A new miniature X-ray device for interstitial radiosurgery: dosimetry. Med Phys 1996;23(1):53–62.
[15] DeWerd LA, Ibbott GS, Meigooni AS, Mitch MG, Rivard MJ, Stump KE, et al. A dosimetric uncertainty analysis for photon-emitting brachytherapy sources: report of AAPM Task Group No. 138 and GEC-ESTRO. Med Phys 2011;38(2):782–801.